To cite this version :

Hussain NOURI, Farid BAKIR, Christophe SARRAF, Florent RAVELET - Experimental investigation on ducted counter-rotating axial flow fans - In: ASME-JSME-KSME 2011 Joint Fluids Engineering Conference, Japan, 2011 - Proceedings of ASME-JSME-KSME Joint Fluids Engineering Conference 2011 - 2011

Experimental investigation on ducted counter-rotating axial flow fans

Hussain NOURI, Florent RAVELET, Farid BAKIR, and Christophe SARRAF

Arts et Metiers ParisTech, DynFluid, 151 boulevard de l'Hôpital, 75013 Paris, France.[a]

An experimental study on counter-rotating axial-flow fans was carried out. The fans of diameter $D = 375$ mm were designed using an inverse method. The counter-rotating fans operate in a ducted-flow configuration and the overall performances are measured in a normalized test bench. The rotation rate of each fan is independently controlled. The distance between the fans can vary from 10 to 50 mm by steps of 10 mm. The results show that the efficiency is strongly increased compared to a conventional rotor or to a rotor-stator stage. The effects of varying the rotation rates ratio on the overall performances are studied and show that the system is highly efficient on a wide range of flow-rates and pressure rises. However, the change of the axial distance between rotors from 10 to 50 mm does not seem to change the overall performances. This system has thus a very flexible use, with a large patch of high efficient operating points in the parameter space. Further local studies including velocity measurements and wall-pressure fluctuations in the space between the rotors are needed to better understand the interactions between the rotors and to optimize the system.

NOMENCLATURE

Subscripts

1	Fan inlet
2	Fan outlet
a	Axial
est	Estimate
m	Mean
r	Radial
s	Static
t	Total
u	Tangential

Roman characters

a	[^{o}]	Angle of attack
c	[mm]	Chord length
$e_\%$	[]	Relative thickness
x/c	[-]	Relative chord wise location
A	[]	Relative axial spacing, S/c
C	[m.s^{-1}]	Flow velocity in the absolute reference frame
$C_{z\infty 0}$	[]	Camber coefficient
D	[mm]	Ducting pipe diameter
S	[mm]	Axial spacing
$\mathcal{D}$	[]	Lieblein's diffusion factor
N	[RPM]	Rotation rate
Q	[$m^3.s^{-1}$]	Flow rate
T	[N.m]	Torque supplied by the shaft
U	[m.s^{-1}]	Moving frame speed
Z	[]	Number of blades
FR	[]	Front rotor
R	[mm]	Blade radius
RR	[]	Rear rotor
CRS	[]	Counter-rotating system
W	[m.s^{-1}]	Flow velocity in the relative reference frame

Greek characters

α	[^{o}]	Flow angle in the absolute reference frame
β	[^{o}]	Flow angle in the relative reference frame
η	[-]	Efficiency
ω	[rad.s^{-1}]	Angular velocity
ϕ	[-]	Flow coefficient
ψ	[-]	Pressure coefficient
γ	[^{o}]	Stagger angle
ρ	[kg.m^{-3}]	Density
σ	[]	Blade solidity
θ	[]	Rotation ratio $\frac{N_{RR}}{N_{FR}}$
Δp	[Pa]	Pressure rise
Ω	[]	Specific speed

[a] Electronic mail: hussain.nouri@paris.ensam.fr

I. INTRODUCTION

Early studied in the 1930's[1,2], the counter-rotating machines arouse a greater interest in the turbomachinery field, particularly for their potential improvement of the efficiency with respect to conventional machines by recovering more kinetic energy from the front rotor exit-flow[3–6]. The first counter-rotating machines have appeared in aeronautic and marine applications, in open configuration. Nowadays, these machines with two coaxial axial-flow fans that rotate in opposite direction see a revival of interest in several distinct configurations —open and ducted flows, shrouded or not shrouded rotors— in various subsonic regime applications.

All previous studies concluded that the presence of the rear rotor improves the global efficiency[3,4] and also increases the operating flow-rate range. The counter-rotating systems (CRS) moreover allow to reduce the fans radial compactness[6]. A CRS requires more axial spacing compared to one simple fan, but not much more than a rotor-stator stage. Another interesting feature of CRS is that it makes it possible to design axial-flow fans with very low specific speed $\Omega = \frac{\omega \sqrt{Q}}{(\Delta p_t/\rho)^{3/4}}$ with ω the mean angular velocity, Q the flow rate, Δp_t the total pressure rise and ρ the fluid density.

With such advantages (radial compactness and efficieny improvement), the CRS becomes a very interesting solution and the interactions between the rotors needs to

be better understood in order to design highly efficient CRS.

The general aim of the present study on ducted counter-rotating axial-flow fans in subsonic regime is to find out a design method of a CRS by investigating the global and the local performances and the interactions between the two rotors. We first present in § II the method that have been used to design the Front and the Rear Rotors. The experimental set-up is presented in § III. Then we report on the overall performances of the system in § IV. The Counter-Rotating system in its default configuration is studied in § IV A and the effects of varying the rotation ratio and the axial spacing between the rotors are presented in § IV B. We then give some conclusive remarks in § V.

II. DESIGN OF THE ROTORS

The design of the rotors is based on the use of the software MFT (Mixed Flow Turbomachinery) developed by the DynFluid Laboratory[7] to which an original method has been added specifically for the design of the Rear Rotor of the Counter-Rotating System.

	CRS	Front Rotor	Rear Rotor
D (mm)	380	380	380
R_{tip} (mm)	187.5	187.5	187.5
R_{hub} (mm)	55	55	55
Z	-	11	7
Δp_t (Pa)	420	260	160
N (RPM)	1900	2000	1800
Q (m^3.s^{-1})	1	1	-
Ω	2.46	3.71	-
Other constraints	Axial exit-flow	Constant vortex	-

TABLE I. Design point of the Counter-Rotating System

The design point of the CRS is given in Tab. I. The system is designed to achieve a total pressure rise $\Delta p_t = 420$ Pa at flow-rate $Q = 1$ m^3.s^{-1} for a mean rotation rate around 1900 rpm. That would correspond to a specific speed $\Omega \simeq 2.46$ which is far too low a value for an axial machine. The dimensions of the system, the number of blades for the Front Rotor (FR) and of the Rear Rotor (RR) and their rotation rates are then imposed. The system that is presented here has moreover been designed to have a pure axial exit-flow. In that case the static pressure rise of the CRS —that is the only pressure rise experimentally accessible— should be $\Delta p_s = \Delta p_t - 1/2\,\rho \left(Q/(\pi D^2/4)\right)^2 \simeq 373$ Pa.

An iterative procedure is then performed. The pressure rise of the Front Rotor is then arbitrarily chosen and FR is designed and quickly analysed as explained in § II A. An estimate of the pressure rise that RR would made is then performed (see § II B), based on this analyse. If the total pressure rise of the CRS is not met, the

design pressure rise of FR is varied and the calculus are made again. The drawback of this method is that the losses and interactions inbetween the two rotors are not taken into account. The effect of the axial spacing S is also not taken into account and is studied in the present Article.

The geometrical characteristics of the rotor blades obtained with this method are summarized in Tab. II. Pictures of the Front and Rear rotors are given in Fig. 1.
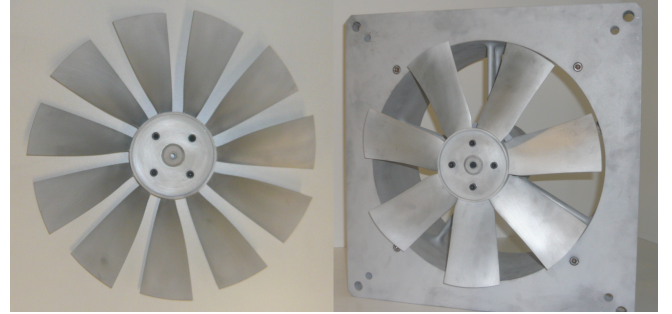

FIG. 1. Picture of the Front Rotor (left) and Rear Rotor (right)

A. Design of the Front Rotor

The Front Rotor (FR) was designed as a conventional fan that meets the specifications reported in Tab. I, i.e. $Q = 1$ m^3.s^{-1}, $\Delta p_{tFR} = 260$ Pa at $N_{FR} = 2000$ rpm. The hub-to-tip radius ratio is $R_{hub}/R_{tip} = 0.293$ with tip radius $R_{tip} = 187.5$ mm. The design is based on the inverse method with simplified radial equilibrium. Rotor is built up from blades of circular-arc camber lines, with NACA-65 profiles clipped at 0.95 x/c. To dimension a new axial machine, the design-point specifications must first be specified (total pressure rise Δp_t, flow rate Q, rotation rate N and radii R_{tip} & R_{hub}). In a second step, the radial distribution of the circumferencial component of the velocity of fluid, $C_{u2}(r)$, is imposed at the rotor outlet (the possible types of vortex model: free, constant, forced or mixed). Assuming a perfect fluid and taking into account a rough estimate of the total efficiency of $\eta_{est} = 60\%$ and the equation of simplified radial equilibrium (radial momentum conservation), the velocity triangles at the inlet and outlet of the rotor can then be defined for each radius. The blades can then be defined by the local resolution of an inverse problem considering a two-dimensional flow and searching for the best suited cascade to the proposed velocity triangles. Precisely, this resolution is possible only if we impose the blade number and the local Lieblein's diffusion factor $\mathcal{D}$ which has an important influence on the optimization criteria. The behavior of the designed machine resulting from the above method can then be analyzed in order to answer the following questions:

Radial position	R	c	σ	γ	profile	$\mathcal{D}$
Front Rotor (blade thickness 4.5 mm)						
Hub	55	40.3	1.28	23	NACA 65(26)11	0.62
Mid-span	121.25	58.0	0.84	57	NACA 65(12)07	
Tip	187.5	75.7	0.71	69	NACA 65(07)06	0.44
Rear Rotor (blade thickness 6 mm)						
Hub	55	58.8	1.18	73	NACA 65(03)10	0.61
Mid-span	121.25	72.9	0.66	65	NACA 65(05)08	
Tip	187.5	87.1	0.51	75	NACA 65(04)07	0.46

TABLE II. Blade cascade parameters for the two rotors. Radius R (mm). Chord length c (mm). Cascade solidity σ. Stagger angle γ (^{o}). Profile designation according to the nomenclature given in Ref.[7]: NACA65(xx)yy with (xx) representing the relative camber and yy standing for the relative thickness. Lieblein's diffusion factor $\mathcal{D}$

- Is the design-point achieved and what are the values of efficiency locally ?

- What are the characteristics of the machine at the neighborhood of the design point ?

For the imposed speed of rotation, the direct method rules are applied in order to determine the velocity triangles corresponding to each flow discharge. The effects due to real fluid are taken partially into account with the introduction of an axial-velocity distribution which considers the boundary layers at the hub and casing. Thus, we can obtain the characteristics of the machine in the vicinity of the design-point discharge.

In the present case, this direct analysis predicts a mean absolute tangential velocity $C_{u2FR} \simeq 9.6$ m.s^{-1} with a radial distribution uniform within $\pm 5\%$ (constant vortex design). The Reynolds number based on the inlet relative velocity varies from 0.6×10^5 at the hub to 3×10^5 at mid-span and 7×10^5 at the tip.

The blades of FR are stacked on the trailing edge in order to ease velocity measurements close to it. Please note that the blades of RR are stacked on the leading edge for the same reasons. The blades have moreover no sweep.

B. Design of the Rear Rotor

The method used for the design of the Rear Rotor (RR) is to considere the velocity and the flow angle at the trailing edge of the FR blades. Therefore, FR was analysed with MFT to retrieve the axial and tangential velocities ($C_{a2FR} = C_{a1RR}$ and $C_{u2FR} = C_{u1RR}$ respectively) and the angle α_{2R1} in the absolute reference frame, at the exit along the blade as shown in Fig. 2.

Using a Matlab script and following an iterative procedure, the RR is drawn in such a way that the exit flow is axial, that is $\alpha_{2RR} = 0^o$. The second hypothesis is that the axial velocity profile is kept constant accross RR, i.e. $C_{a2RR}(r) = C_{a1RR}(r)$. Under these assump-
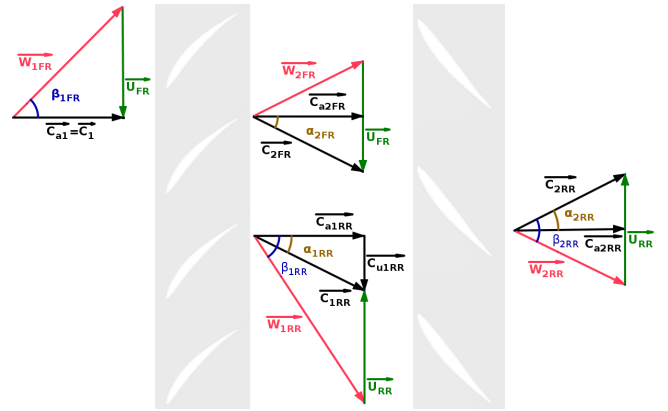

FIG. 2. Velovity Triangles for the CRS. The fluid is flowing from left to right. Please see the Nomenclature for the meaning of the capital letters and subscripts. Please also note that this is a general case where the exit-flow is not constrained to be solely axial

tions, the total pressure rise of RR should be $\Delta p_{tRR} = \eta_{est} \, \rho \, U_{mRR} \, C_{u2FR} \simeq 0.6 \times 1.2 \times 22.9 \times 9.6 \simeq 160$ Pa.

In order to completely define the geometry of the blade cascade, we have to compute γ the stagger angle, σ the solidity, c the chord, $e_{\%}$ the relative thickness and $C_{z\infty 0}$ the camber coefficients. This inverse problem is solved with the following empirical equations that have been validated for NACA-65 cascades[7], for $0.5 \leq \sigma \leq 1.5$ and $0 \leq C_{z\infty 0} \leq 2.7$:

$$\gamma = \beta_{1RR} - a, \qquad (1)$$

a is the angle of attack and is obtained by:

$$a = \frac{\Delta \beta_{RR} + 0.94}{q(\beta_{1RR})} + 2.07 \qquad (2)$$

with q(β_{1RR}) defined by:

$$q(\beta_{1RR}) = 2.103 - 4.019 10^{-7} \beta_{1RR}^{3.382} \qquad (3)$$

The solidity σ is computed by:

$$\sigma^{-1} = \left(\mathcal{D} - 1 + \frac{C_{2RR}}{C_{1RR}} \right) \times \left(\frac{2C_{1RR}}{|\Delta C_{uRR}|} \right) \qquad (4)$$

with $\mathcal{D}$ the Lieblein's diffusion factor. The solidity is computed at the hub and at the tip with $\mathcal{D}_{hub} = \mathcal{D}_{tip} = 0.5$ as initial values. Then equation 5 is used to obtain the chord at the hub and the tip:

$$c = \sigma \frac{2\pi R}{Z} \qquad (5)$$

where Z is the number of blades. The chord is computed at the tip and at the hub then the intermediate chords are obtained by linearization. The maximum thickness was set to $e_{max} = 6$ mm. Finally, the camber coefficients $C_{z\infty 0}$ are computed by:

$$C_{z\infty 0} = \frac{a + 2.525}{p(\sigma)} - 0.823 \qquad (6)$$

where

$$p(\sigma) = 15.535 - 12.467 e^{-0.4242\sigma} \qquad (7)$$

We then check that the solidity lays in the range $0.5 \leq \sigma \leq 1.5$ and that the camber lays in the range $0 \leq C_{z\infty 0} \leq 2.7$. After several iterations, the RR was drawn with $\mathcal{D}_{hub} = 0.61$ and $\mathcal{D}_{tip} = 0.46$.

III. EXPERIMENTAL SET-UP

The Counter-Rotating System is studied in a ducted-flow test rig —AERO^{2}FANS— that has been built according to the ISO-5801 standards[8,9]. The Figure 3 shows this test rig. It consists of a cylindrical pipe of inner diameter $D = 380$ mm. A bell mouth is flush-mounted at the inlet of the duct to reduce the energy loss due to fluid friction and flow separation of the inlet flow. The upstream face of FR is at a distance $5D$ from the pipe inlet. A honeycomb is placed upstream of FR to homogenize the incoming flow. Two brushless PANASONIC A4 motors drive each rotor separately and are hidden in a casing of diameter $0.33D$ and of length $0.45D$, with a warhead-shape end. For the front motor the honeycomb ensures the binding to the tube. The rear motor is bound to the tube by two rod rows (3 and 5 rods, the first row being at $0.1D$ from the Rear Rotor). An anti-gyration device made of eight metal sheets of thickness 1.5 mm and length $2D$ is placed $2D$ downstream of the CRS. It prevents the outgoing flow from having

any rotating component and the static pressure evaluated downstream is more reliable. The static pressure of the axial fan is measured $1D$ downstream of the anti-gyration device, with an average over four flush-mounted pressure taps. To make the installation more compact, a tube bend of 180° is placed $1D$ downstream of the pressure taps. The flow rate is measured with a normalized diaphragm, located $10D$ downstream of the tube bend and $5D$ upstream of the pipe outlet. The diaphragm has a diameter of $0.73D$. An iris damper —originally used for air flow regulation in ducts— is placed at the exit of the pipe to vary the test-bench hydraulic impedance and thereby to vary the operating point of the studied axial-flow fan. Finally, an axial blower can also be used at the exit of the pipe to widen the explored flow-rate. The static pressure losses from the honeycomb, the motors casings and the anti-gyration device have been measured using this axial blower and have been added to the static pressure rise measurements.

The study focuses on the influence of the gap between the rotors (axial spacing S) as well as on the influence of the speed ratio $\theta = \frac{N_{RR}}{N_{FR}}$. The axial spacing vary from $S = 10$ mm to $S = 50$ mm by steps of 10 mm. Clear Plexiglas blocks of different thickness are used to change the axial spacing. The reason of using transparent material is to allow forthcoming optical measurements of the velocity field with Laser Doppler Anemometry (LDA) or Particle Image Velocimetry (PIV). Unless specified the default axial spacing is $S = 10$ mm. Regarding the speed ratio, each rotor is driven separately so all combinations are possible. The default configuration is $\theta = 0.9$ (see Tab. I).

IV. RESULTS AND DISCUSSION

A. Overall performances of the reference system ($\{\theta = 0.9 \,;\, S = 10\mathbf{mm}\}$)

The characteristics of the Front Rotor rotating alone (RR has been removed from its shaft in that case), of the Rear Rotor rotating alone (FR has been removed) and of the Counter-Rotating system are shown in Fig. 4. The operating speeds are the design speeds, *i.e.* 2000 rpm for the Front Rotor and 1800 rpm for the Rear Rotor. The static efficiency is defined by equation 8:

$$\eta_s = \frac{\Delta P_s Q}{(T_{FR}\omega_{FR}) + (T_{RR}\omega_{RR})} \qquad (8)$$

The nominal flow-rates of the three systems, *i.e.* the flow-rates at maximum efficiency, are reported in Tab. III together with the corresponding static pressure rises and efficiencies.

The Front Rotor rotating alone has a very flat curve (red □ in Fig. 4). The characteristic curve could not be explored for flow-rates higher than 3800 m^3.h^{-1}, *i.e.*
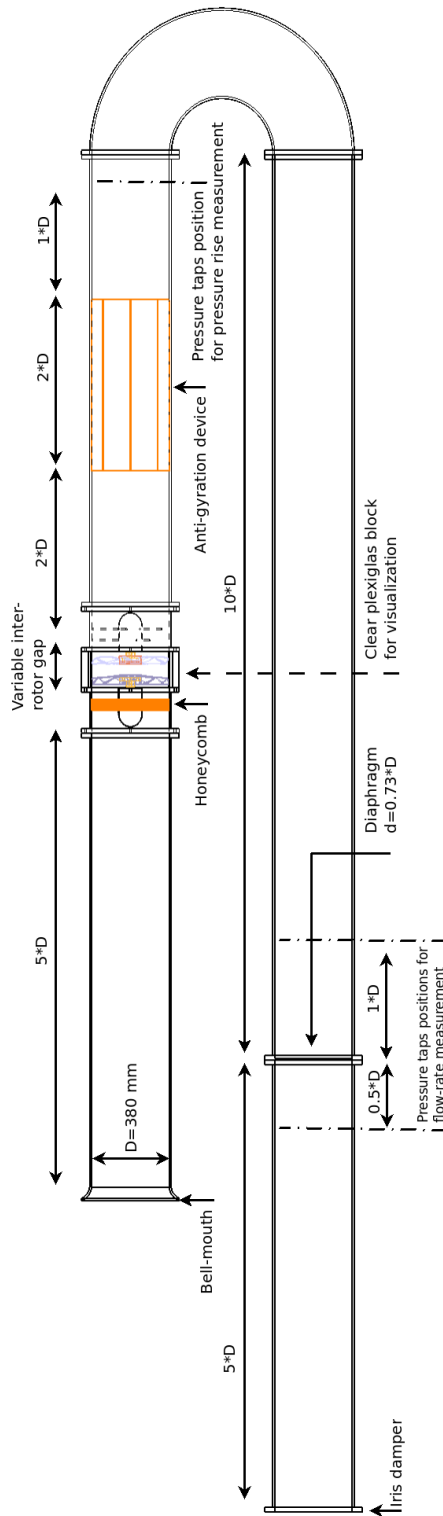
FIG. 3. Experimental facility for CRS, $AERO^2FANS$

FIG. 4. Fans characteristics: (a) static pressure rise Δp_s *vs* flow rate Q; (b) static efficiency η_s *vs* flow rate Q. The axial spacing is $S = 10$ mm. Red $\square$: FR rotating alone at $N_{FR} = 2000$ rpm (RR has been removed), blue $\star$: RR rotating alone at $N_{RR} = 1800$ rpm (FR has been removed) and black $\circ$: CRS at $N_{FR} = 2000$ rpm and $\theta = 0.9$. The blue $\blacksquare$ and the dashed lines stand for the design point of the CRS

	Front Rotor	Rear Rotor	CRS
Maximum efficiency (%)	45.28	54.48	64.73
nominal Q (m^3.s^{-1})	1.03	0.71	0.99
Δp_s (Pa)	148	90	340

TABLE III. Nominal points of FR rotating alone at $N_{FR} = 2000$ rpm, RR rotating alone at $N_{RR} = 1800$ rpm and CRS at $N_{FR} = 2000$ rpm and $\theta = 0.9$ (see also Fig. 4)

1.06 m^3.s^{-1}, even with the help of the blower. The nominal flow-rate of FR is slightly greater than the design point —it is 3% greater. The measured static pressure rise at the design point is 148 Pa, with a rela-

tively low static efficiency of 45%. This is not surprising with no shroud and a large radial gap of 2.5 mm. Numerical analysis performed with MFT[7] and with Fluent 6.3 give very similar results for the static pressure rise $(142 \leq \Delta p_s \leq 153$ Pa). The total pressure rise predicted by these two different numerical methods —a model using semi-empirical correlations *vs* Computational Fluid Dynamics— is roughly 260 Pa. The predicted global performances of FR can thus be considered as validated. The remaining question is about the prediction of the exit-flow velocity components, *i.e.* of the exit-flow angles. This question could of course only be answered with systematic and deep velocity measurements that are scheduled. However, the present global measurements could

give partial informations.

The Rear Rotor rotating alone has a steeper curve (blue ★ in Fig. 4) and its nominal flow-rate $Q \simeq 2600$ m^3.h^{-1} is lower than the design flow-rate of FR and CRS. This is consistent with the bigger stagger angle of the blades (see Tab. II).

Let us examine the velocity triangles in Fig. 2 and consider the case with the Front coupled to the Rear Rotor: the incoming velocity $C_{1RR}=C_{2FR}$ has an axial component as well as a tangential component. Hence, the flow angle in the relative reference frame reads:

$$tan(\beta_{1RR}) = \frac{U_{RR} + C_{u1RR}}{C_{a1RR}} \quad (9)$$

Let us consider now the case without the Front Rotor and assume that the flow through the honeycomb is axial. Since the tangential component does not exist anymore and the incoming velocity has only the axial component, equation 9 becomes:

$$tan(\beta_{1RR}) = \frac{U_{RR}}{C_{a1RR}} \quad (10)$$

Let us now compute the result of equation 9 for the mean radius and at the nominal flow-rate of the CRS, asuming that the tangential velocity is well predicted by MFT, that is $\langle U_{RR} \rangle \simeq 22.9$ m.s^{-1}, $\langle C_{a1RR} \rangle \simeq 8.8$ m.s^{-1} and $\langle C_{u1RR} \rangle = \langle C_{u2FR} \rangle \simeq 9.6$ m.s^{-1}. This leads to $\langle tan(\beta_{1RR}) \rangle \simeq 3.69$. If we now suppose that RR rotating alone has its maximum efficiency when the tangent of the inlet flow-angle is equal to this value, equation 10 implies that this is for a flow-rate such that $\langle C_{a1RR} \rangle = \frac{\langle U_{RR} \rangle}{tan(\langle \beta_{1RR} \rangle)} \simeq 6.2$ m.s^{-1}, $i.e.$ $Q \simeq 0.705$ m^3.s^{-1} or 2540 m^3.h^{-1}. This is exactly the nominal flow-rate of RR rotating alone (see Fig. 4 and Tab. III). The estimations of the angles behind the Front Rotor using the direct analysis of MFT thus seem consistent.

The characteristic curve of the CRS (black ∘ in Fig. 4) is steeper than the characteristic curve of FR. It is roughly parallel to the RR curve. The nominal flow-rate of the CRS matches well with the design flow-rate, $i.e.$ 1 m^3.s^{-1}. The static pressure rise at the nominal discharge ($\Delta p_{sCRS} = 340$ Pa) is 10% lower than the design point (373 Pa), which is not so bad in view of the rough approximations used to design the system. The CRS has a high static efficiency ($\eta_{sCRS} = 65\%$) compared to a conventional axial-flow fan or to a rotor-stator stage with similar dimensions, working at such Reynolds numbers[10,11]. The gain in efficiency with respect to the Front Rotor is 20 points, whilst an order of magnitude of the maximum gain using a stator is typically 10 points[10,11].

The flow-rate range for which the static efficiency lays in the range $60\% \leq \eta_s \leq 65\%$ is: $2750 \lesssim Q \lesssim 4150$ m^3.h^{-1}, that is from 76% of the nominal flow-rate up to 115% of the nominal flow-rate. One open question is to what extent the global performances of the CRS are affected by the axial spacing and the speed ratio, and whether the efficient range could be extended by varying the speed ratio.

B. Influence of the rotation ratio θ and of the axial spacing S
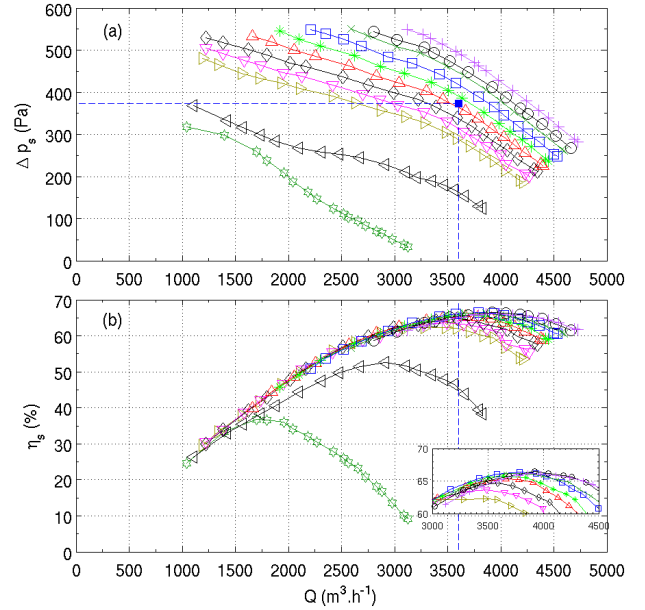
Rotation ratio θ

FIG. 5. CRS characteristics at $N_{FR} = 2000$ rpm, $S = 10$ mm and $\theta \in [0\,;1.2]$: (a) static pressure rise Δp_s vs flow rate Q; (b) static efficiency η_s vs flow rate Q. Dark green ✿: $\theta = 0$, black ◁: $\theta = 0.5$, mustard yellow ▷: $\theta = 0.8$, magenta ▽: $\theta = 0.85$, cyan ◇: $\theta = 0.9$, red △: $\theta = 0.95$, green ∗: $\theta = 1$, blue □: $\theta = 1.05$, dark green ×: $\theta = 1.1$, black ∘: $\theta = 1.15$ and purple +: $\theta = 1.2$. The blue ■ and the dashed lines stand for the design point of the CRS
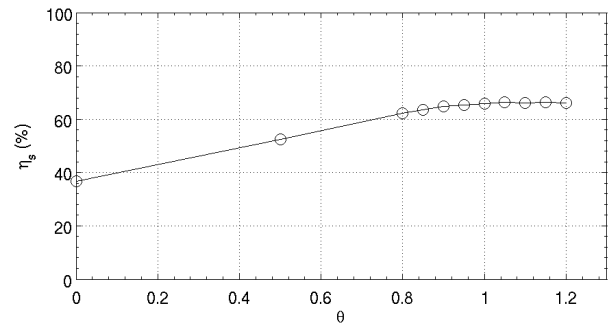

FIG. 6. Maximal static efficiency η_s vs θ for the CRS with $N_{FR} = 2000$ rpm and $S = 10$ mm

In this paragraph, the rotation rate of FR is kept constant at N_{FR} = 2000 rpm, and the rotation rate of RR is varied from 0 rpm to 2400 rpm. The corresponding θ are $\theta = \{0\,;\,0.5\,;\,0.8\,;\,0.85\,;\,0.9\,;\,0.95\,;\,1\,;\,1.05\,;\,1.1\,;\,1.15\,\&\,1.2\}$. The axial spacing is $S = 10$ mm.

The overall performances of the CRS in these conditions are plotted in Fig. 5. As expected, the more the rotation rate of RR increases, the more the static pressure rise of the CRS increases and the nominal flow-rate of the CRS increases. The maximal efficiency as a function of θ is plotted in Fig. 6.

For very low rotation rates of RR, *i.e.* for $\theta = 0$ (Dark green ✩ in Fig. 5) and $\theta = 0.5$ (black ◁ in Fig. 5), the system is very unefficient: in the first case when the RR is at rest the maximum efficiency hardly reaches 35% which is below the maximal efficiencies of both FR and RR alone. The maximum flow-rate that can be reached is moreover very low in both cases compared to the discharge goal of 3600 m^3.h^{-1}.

In the range $\theta \in [0.8\,;\,1.2]$, *i.e.* $N_{RR} \in [1600\,;\,2400]$ rpm, the system is highly efficient. The maximum efficiency increases with θ to reach a maximum value of 66.5% for $\theta = 1.05$ and is then quasi-constant ($\eta_s = 66.0\%$ for $\theta = 1.20$).

This is a very interesting feature of the Counter-Rotating System. One could imagine, simply by varying the Rear Rotor rotation rate, to work at a constant pressure rise with an efficiency greater than 60% for a large flow-rate range. For instance in the present case, the system could give a constant static pressure rise of 375 Pa with $\eta_s \geq 60\%$ for $3000 \leq Q \leq 4250$ m^3.h^{-1} with $N_{FR} = 2000$ rpm, $S = 10$ mm and $\theta \in [0.85\,;\,1.2]$.

One could also imagine to work at a constant flow-rate with high static efficiency. For instance in the present case, the system could give a constant flow-rate of 3600 m^3.h^{-1} with $\eta_s \geq 60\%$ for $290 \leq \Delta p_s \leq 490$ Pa with $N_{FR} = 2000$ rpm, $S = 10$ mm and $\theta \in [0.8\,;\,1.2]$.

Axial spacing S

Four axial spacings were studied: $S = 10, 20, 40\,\&\,50$ mm. Figure 7 shows the characteristics curves at the design rotation rates, i.e., $N_{FR} = 2000$ rpm and $\theta = 0.9$. For this range of axial distances, the overall performances do not vary a lot. There is a slight tendency to a decrease in performance with increasing distances: at the design flow-rate, the difference in static pressure between the best case ($S = 10$ mm) and the worst case ($S = 40$ mm) is 17 Pa, which corresponds to a relative decrease of 5%. The efficiency does not vary significantly either. In other studies[3,4] it was reported that the axial spacing had a more significant influence on the overall performances. This is probably due to a difference in the axial distance range.

Let us take as a significant length scale the mean chord length of the Front Rotor ($c_{FR} = 58$ mm). We introduce
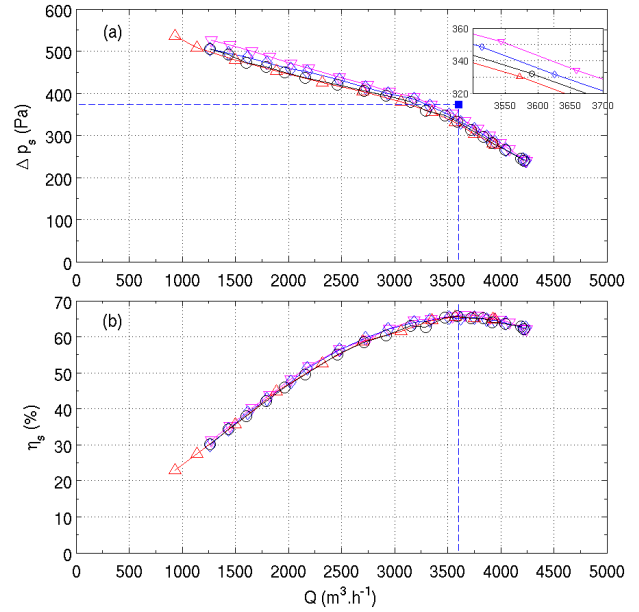

FIG. 7. CRS characteristics at various axial spacing: (a) static pressure rise Δp_s *vs* flow rate Q; (b) static efficiency η_s *vs* flow rate Q. The rotation ratio of FR is $N_{FR} = 2000 rpm$ and $\theta = 0.9$. Magenta ▽: $S = 10\ mm$, blue ◇: $S = 20\ mm$, red △: $S = 40\ mm$ and black ○: $S = 50\ mm$. The blue ■ and the dashed lines stand for the design point of the CRS

the relative axial spacing A:

$$A = \frac{S}{c_{FR}} \qquad (11)$$

The results reported here concern the range $A \in [0.17\,;\,0.86]$. The latter value of A is probably too small to see a significant decrease in performances. The effects reported in[3,4] were indeed significant for $A = 2$. Further studies with greater values of A are scheduled. The effects of the axial spacing on the level of pressure fluctuations will also be investigated in future works.

V. CONCLUSION

A Counter-Rotating axial-flow fan has been designed according to an iterative method that is relatively fast. It is based on semi-empirical modelization that partly takes into account the losses, boundary layers at hub and casing, and the effects of "low" Reynolds numbers (below 2×10^5).

The overall performances at the nominal design point are slightly lower than predicted, with a static pressure rise 10% lower. The static efficiency is however remarkably high ($\eta_s \simeq 65\%$) and corresponds to a 20 points gain in efficiency with respect to the Front Rotor maximal efficiency and to a 10 points gain with respect to the

Rear Rotor. The overall measurements give first clues that allow to validate the design method.

The Counter-Rotating System has a very flexible use that allows to work at constant flow-rate on a wide range of static pressure rises or to work at constant pressure rise on a wide range of flow-rates, with static efficiency bigger than 60%, simply by varying the Rear Rotor rotation rate. One could thus imagine an efficient closed-loop-controlled axial-flow fan. The overall performances moreover do not significantly vary with the axial spacing in the range $A \in [0.17 ; 0.86]$. This range will be extended to at least 2 Front Rotor chords.

Local measurements of the velocity field in the wake of the Front Rotor rotating alone are scheduled, in order to confirm the design. These measurements will also be of great interest concerning the understanding of the interaction in the space betwenn the rotors. Local measurements of wall-pressure fluctuations are planed, and may show a greater influence of the axial spacing.

The authors finally wish to thank Robert Rey for very fruitfull discussions.

[1] Lesley, E., 1933. Experiments with a counter-propeller. Tech. Rep. 453, National Advisory Committee for Aeronautics.

[2] Lesley, E., 1939. Tandem air propellers. Tech. Rep. 689, National Advisory Committee for Aeronautics.

[3] Sharma, P., Jain, Y., and Pundhir, D., 1988. "A study of some factors affecting the performance of a contra-rotating axial compressor stage". *Proceedings of the Institution of Mechanical Engineers. Part A. Power and process engineering,* **202**, pp. 15–21.

[4] Sharma, P., Pundhir, D., and Chaudhry, K., 1991. "A study of aeroacoustic performance of a contra-rotating axial flow compressor stage". *Def Sci J,* **41**, pp. 165–180.

[5] Min, K.-S., Chang, B.-J., and Seo, H.-W., 2009. "Study on the contra-rotating propeller system design and full-scale performance prediction method". *International Journal of Naval Architecture and Ocean Engineering,* **1**, pp. 29–38.

[6] Shigemitsu, T., Furukawa, A., Watanabe, S., Okuma, K., and Fukutomi, J., 2009. "Internal flow measurement with ldv at design point of contra-rotating axial flow pump". *Journal of Fluid Science and Technology,* **4**, pp. 723–734.

[7] Noguera, R., Rey, R., Massouh, F., Bakir, F., and Kouidri, S., 1993. "Design and analysis of axial pumps". In ASME Fluids Engineering, Second Pumping Machinery Symposium, Washington, USA., pp. 95–111.

[8] ISO, 2007. *ISO 5801 - Industrial fans Performance testing using standardized airways.* International Standards for Business, Government and Society.

[9] Sarraf, C., Nouri, H., Ravelet, F., and Bakir, F., 2011. "Experimental study of blade thickness effects on the global and local performances of a controlled vortex designed axial-flow fan". *Experimental Thermal and Fluid Science,* **doi:10.1016/j.expthermflusci.2011.01.002**.

[10] Moreau, S., and Bakir, F., 2002. "Efficient stator designed for automotive engine cooling fan systems". In ASME 2002 Fluids Engineering Division Summer Meeting, pp. FEDSM02–31318.

[11] Bakir, F., and Moreau, S., 2003. "Detailed study of an efficient small diameter automotive engine cooling fan system". In ASME 2003 Fluids Engineering Division Summer Meeting, pp. FEDSM2003–45117.